University of the Philippines Baguio, , Philippines, 2014、招待

Miyazawa K. Growth of fullerene nanowhiskers by LLIP method. Collaborative Conference on Crystal Growth 3CG 2014, Phuket, Thailand, 2014、招待.

D. Matsuura, T. Konno, T. Wakahara, K. Miyazawa, T. Kizuka, "Young's modulus of $C_{60}/C_{70}$ alloy nanowhiskers", 2014 Tsukuba Nanotechnology Symposium (TNS'14), July 25-26, 2014, University of Tsukuba, Tsukuba, Japan.

Miyazawa K, Hirata C, Wakahara T. Controlled growth of $C_{60}$ fullerene nanowhiskers, Fifteenth International Symposium on Biomimetic Materials Processing (BMMP-15), Nagoya、招待

宮澤薫一:強制混合 LLIP 法におけるフラーレンナノウィスカー結晶核の生成に関する考察. 日本物理学会第 70 回年次大会;東京、2015.

今野俊生、若原孝次、宮澤薫一: $C_{60}$-$C_{70}$2 成分ナノウィスカーの合成と構造解析(3). 日本物理学会第 70 回年次大会;東京、2015.

菅野 純、評価と管理の分界に関する考察、平成 26 年度日本環境変異原学会公開シンポジウム( 2014. 5.24)東京

酒々井真澄、沼野琢旬、深町勝巳、二口充、津田洋幸(2014)カーボンナノチューブの中皮腫発がんプロファイル;第41回日本毒性学会学術年会 神戸 7 月 2 日−4 日

Suzui M., Sato K., Isoda Y., Numano T., Futakuchi M., Fukamachi K., Xu J., Tsuda H., (2014) Carcinogenic profile of carbon nanotubes on the rat lung 第 73 回日本癌学会総会 横浜 9 月 25-27 日

酒々井真澄、沼野琢旬、深町勝巳。二口充、津田洋幸(2015)多層カーボンナノチューブの腫瘍発生プロファイル;第31回日本毒性病理学会総会 東京 1 月 29 日-30 日

津田洋幸、徐結旬、Alexander D.B.,酒々井真澄、二口充、深町勝巳、広瀬明彦、菅野純 (2015) 多層カーボンナノチューブの発がん標的性組織;第 14 回分子予防環境医学研究会大会 大阪, 2 月 13 日−2 月 14 日.

小林憲弘, 田中亮太, 竹原広, 納屋聖人, 久保田領志, 五十嵐良明, 広瀬明彦:マウス反復気管内投与による多層カーボンナノチューブの催奇形性の評価. 第 41 回日本毒性学会学術年会 (2014.7.2 兵庫県神戸市).

Yuhji Taquahashi, Yukio Ogawa, AtsuyaTakagi, Masaki Tsuji, Koichi Morita, Jun Kanno, An Improved Dispersion Method (Taquann Method) of Multi-wall CarbonNanotube for a Whole Body Inhalation Exposure System,53rd SOT (2014,3,Phoenix)

Jun Kanno, An Improved Dispersion Method (Taquann Method) of Multiwall Carbon Nanotube for a Whole-Body Inhalation Exposure System, . the 53rd Annual Meeting of the Society of Toxicology (2014.3.26) Phoenix, USA, poster

菅野 純、炎症と癌 - 異物発癌としての中皮腫繊維発癌からの考察 - 、平成 25 年度「個

体レベルでのがん研究支援活動」ワークショップ、(2014.2.17)、大津、基調講演

高橋 祐次、小川 幸男、高木 篤也、辻 昌貴、森田 紘一、菅野 純、多層カーボンナノチューブの p53+/-マウス全身暴露吸入実験、平成 25 年度「個体レベルでのがん研究支援活動」ワークショップ、2014 年 2 月 18 日、大津、

菅野 純、高橋祐次、多層カーボンナノチューブの中皮腫発がん性をモデル標的としたナノマテリアル高度分散全身吸入 Taquann システムによるマウス吸入毒性病変評価、第 30 回日本毒性病理学会総会および学術集会、(2014.1.31)、徳島、シンポジウム

坂本義光、小縣昭夫、湯澤勝弘、久保喜一、安藤弘、長澤明道、高橋博、矢野範男、西村哲治、広瀬明彦、井上義之、橋爪直樹、猪又明子、中江 大 "ラットにおいて多層カーボンナノチューブの経気管噴霧反復投与が及ぼす影響" 第30回 日本毒性病理学会 2014. 1. 徳島

Akihiko Hirose, Norihiro Kobayashi, Tomoko Fujitani, Yoshimitsu Sakamoto, Yasuo Yoshioka, Yasuo Tsutsumi, Hiroyuki Tsuda, Jun Kanno : Nanotoxicity and nano safety science in various exposure scenarios. (Symposium invited) EUROTOX2013 (2013.9, Switzerland, Interlaken)

Jun Kanno, Nanotoxicology-its chronic aspects, 6th International Symposium on Nanotechnology, Occupational and Environmental Health (NanOEH2013), Lecture from organizer (2013.10, Nagoya)

Yuhji Taquahashi, Yukio Ogawa, Atsuya Takagi, Masaaki Tsuji, Koichi Morita, Jun Kanno, An Improved Dispersion Method of MWCNT for Whole Body Inhalation Exposure System, 6th International Symposium on Nanotechnology, Occupational and Environmental Health (NanOEH2013) , (2013.10, Nagoya)

菅野 純、ナノマテリアル安全性評価の進捗ー発がん性に関わる知見を中心にー、第 20 回 がん予防学会、2013 年 7 月、東京、シンポジウム

菅野 純、高橋祐次、ナノマテリアルの高分散小型全身曝露吸入システムの開発、第 40 回 日本毒性学会学術年会、2013 年 6 月、千葉、シンポジウム

坂本義光、小縣昭夫、猪又明子、西村哲治、広瀬明彦、中江 大"繊維長の異なる多層カーボンナノチューブによるラット中皮腫誘発性の検討"第40回日本毒性学会2013.6, 幕張

藤谷知子、安藤弘、久保喜一、猪又明子、小縣昭夫、広瀬明彦、西村哲治、中江大:マウスにおけるナノマテリアルの催奇形性に関する研究。第40回日本毒性学会学術年会、2013, 6,17-19, 幕張

小林憲弘、沼野琢旬、中島弘尚、河部真弓、久保田領志、広瀬明彦:妊娠マウスを用いた気管内投与による多層カーボンナノチューブの生殖・発生毒性の評価、第 40 回日本毒性学会学術年会、2013, 6,17-19, 幕張

山本行男、坂本義光、大貫文、猪又明子、小縣昭夫、広瀬明彦、中江大:多層カーボンナノチューブ(MWCNT)投与による中皮

腫誘発ラットにおけるプロテオーム解析(第三報):形状の異なるMWCNT投与ラットにおける血清タンパク質の発現変動。第86回日本生化学会大会、2013, 9,11-13, 横浜

Sakamoto Y, Ogata A, Nishimura T, Hirose A, Nakae D.Induction of mesothelioma by an intraperitoneal administration of 7 different manufactured multi-wall carbon nanotubes.72 th Annual Meeting of the Japanese Cancer Association ; Yokohama, 2013,10

Akihiko Hirose, Norihiro Kobayashi, Mayumi Kawabe*1, Hironao Nakashima*1, Takamasa Numano*1*2, Reiji Kubota, Yoshiaki Ikarashi: Developmental toxicity by intratracheal instillation of multi-wall carbon nanotubes in pregnant mice. 6th International Symposium Nanotechnology, Ocupational and Environmental Health (2013.10, Nagoya)

Kobayashi N, Kawabe M, Nakashima H, Numano T, Kubota R, Sugimoto N, Hirose A: Evaluation of reproductive and developmental toxicity of multi-wall carbon nanotubes in pregnant mice after intratracheal instillation. 52nd Annual Meeting of the Society of Toxicology (SOT2013) (2013, San Antonio)

Nishimaki-Mogami, T., Cui, H., Wu, W., Okuhira, K., Naito, M., Nishimura, T., Sakamoto, Y., Ogata, A., Maeno, T., Inomata, A., Nakae, D., Miyazawa, K., Hirose, A. High-temperature calcined fullerene nanowhiskers and multi-wall carbon nanotubes have abilities to induce IL-1beta secretion through NLRP3-dependent mechanism, depending on their lengths. EUROTOX 2013 (9.3) (Interlaken, Switzerland)

Yamada K, Iwasa A, Kondo T, Kurosawa M, Arakaki R, Yamada A, Kudo Y, Taquahashi Y, Takagi A, Kanno J, Ishimaru N: Invivo effect of multi-wall carbon nanotubes on immune system. 6th International Symposium on Nanotechnology, Occupational and Environmental Health. Nov. 2013 Nagoya

二口充, 徐結苟, 深町勝巳, 津田洋幸,酒々井眞澄. ナノ材料の噴霧曝露後、長期間経過して発生するリスクの背景となる肺組織の検索. 第40回日本毒性学会学術年会, (2013),6月17日-19日,千葉

Suzui, M., Ikenaga, S., Isoda, Y., Numano, T., Fukamachi, K., Futakuchi, M., and Tsuda, H. (2013). Inflammation profile and gene expression status induced by intratracheal instillation of the multiwall carbon nanotube into rat lung. The XIII International Congress of Toxicology 2013 Seoul, Korea, June 30. - July 34.

Numano, T., Ikenaga, S., Isoda, Y., Fukamachi, K., Futakuchi, M., and Suzui, M., Inflammation profile and gene expression status induced by

intratracheal instillation of the multiwall carbon nanotube. 72nd Annual Meeting of the Japanese Cancer Association Yokohama, (2013)Oct. 3. - Oct. 5.

Xu, J., Alexander, DB., Iigo, M., Takahashi, S., Yokoyama, T., Kato, M., Usami, I., Tokuyama, T., Tsutsumi, M., Tamura, M., Oguri, T., Niimi, A., Hayasho, Y., Yokoyama, Y., Tonegawa, K., Fukamachi, K., Futakuchi, M., Suzui, M., Kamijima, M., Hirose, A., Kanno, J., and Tsuda, H. CCL3 as a serum biomarker bfor asbestos exposure and possible biomarker for malignant mesothelioma, The 72th Annual Meeting of the Japanese Meeting of Cancer Association, Yokohama(2013)

Xu, J., Futakuchi, M., Alexander, DB., Fukamachi, K., Suzui, M., Kanno, J., Hirose, A. and Tsuda, H. Dissolution of nano-ZnO is responsible for reversible epithelial hyperplasia of terminal bronchioles. (P-02-41). The 6th International Symposium on Nanotechnology, Occupational and Environmental Health, October 28-31, 2013, Nagoya, Japan.

Xu, J., Alexander, DB., Futakuchi, M., Numano, T., Fukamachi, K., Suzui, M. and Tsuda, H. Size- and shape-dependent pleural transloction, deposition and fibrogenesis by MWCNT dosed to the rat lung. (WS2-2). The 30th Annual Meeting of the Japanese Society of Toxicologic Pathology, January 30-31, 2014, Tokushima, Japan.

Tsuda, H., Xu, J., Alexander, D.B., Tokuyama, T., Usami, I., Hayashi, Y., Oguri, T., Takahashi, S. and Suzui, M. CCL3 as a serum biomarker for asbestos exposure and malignant mesothelioma. (WS1-4). The 30th Annual Meeting of the Japanese Society of Toxicologic Pathology, January 30-31, 2014, Tokushima, Japan.

Xu, J., Alexander, DB., Kanno, J., Hirose, A. and Tsuda, H. Size- and shape-dependent toxicokinetics and fibrogenesis of MWCNT. OECD Expert Meeting on Toxicokinetics of Nanomaterials, February 25-28, 2014, Seoul, Republic of Korea.

Norihiro Kobayashi, Takamasa Numano, Reiji Kubota, Yoshiaki Ikarashi, Akihiko Hirose: Developmental toxicity assessment of multi-wall carbon nanotubes in pregnant mice after intratracheal instillation. 53rd Annual Meeting of the Society of Toxicology (SOT 2014) (2014.3.24 Phoenix, AZ, USA).

橋口誠子、吉田裕樹、徳田健治、紺野克彦、広瀬明彦、黒川昌彦、渡辺　渡　多層型カーボンナノチューブ曝露による RS ウィルス感染免疫への影響、第 61 回日本ウィルス学会学術集会、2013.11.10, 大阪、ポスターP1-032

橋口誠子、吉田裕樹、徳田健治、紺野克彦、

明石　敏、広瀬明彦、黒川昌彦、渡辺　渡
多層型カーボンナノチューブ曝露による
RS ウィルス感染免疫への影響、日本薬学
会第 134 年会、2014.2.28, 熊本、ポスタ
ー28pmS-064

今野俊生, 若原孝次, 宮澤薫一, “C60-C702
成分ナノウィスカーの合成”, ナノファイバ
ー学会第4回年次大会講演予稿集,P.26,
2013 年 7 月 5 日, つくば

D. Matsuura, C. Hirata, T.Konno,
T.Wakahara, K. Miyazawa, T. Kizuka,
“In Situ Transmission Electron
Microscopy of Bending Process of
C60/C70 Nanowhiskers”, Abstracts of
APPC12, The 12th Asia Pacific
Physics Conference, pp. 865-865,
2013 年 7 月 14-19 日,千葉

T. Konno, T.Wakahara and K. Miyazawa,
"Synthesis and Structural Analyses of
C60-C70 Two-Component Fullerene
Nanowhiskers", Abstracts of 23rd
Annual Meeting of MRS-Japan 2013,
P.J-O9-006, Dec. 9-11, 2013, Yokohama
Port Opening Plaza, Yokohama

Kun'ichi Miyazawa, Chika Hirata, Toshio
Konno, Takatsugu Wakahara,
Ryosuke Kano,Masaru Tachibana,
"Synthesis of C60-C70 two-component
fullerene nanowhiskers by LLIP
method", nanoeh6abs program,
P.28-28, 6th International Symposium
on Nanotechnology, Occupational and
Environmental Health, Nagoya
Congress Center, October 28 - 31, 2013,
Nagoya

今野俊生, 若原孝次, 宮澤薫一, “C60-C702
成分ナノウィスカーの合成と構造解析”, 日
本物理学会講演概要集, 第68巻第2号第
4分冊, P.740, 2013年秋季大会, 2013年
9月25日～9月28日, 徳島

松浦大輔, 今野俊生, 若原孝次, 宮澤　薫
一, 木塚徳志, “C60/C70 合金ナノウィスカ
ーのヤング率の組成依存性”, 2014 年春
期講演大会(第 154 回)日本金属学会講
演大会概要集, P.22, 2014 年 3 月 21 日
～23 日, 東京

高橋祐次、高木篤也、辻　昌貴、菅野　純、
p53+/-マ ウスを用いた多層カーボンナノ
チューブの中皮腫発癌評価、個体レベル
でのがん研究支援活動ワークショップ、
2013 年 2 月、大津、ポスター

坂本義光, 小縣昭夫, 西村哲治, 広瀬明彦,
猪又明子, 中江大. ラットにおける多層カ
ーボンナノチューブによる中皮腫誘発性に
繊維長が及ぼす影響. 第 29 回日本毒性
病理学会; つくば, 2013

Jun Kanno, Atsuya Takagi, Yuhji
Taquahashi, Akihiko Hirose,
Nanotoxicology - its chronic aspects,
Workshop on the risk management of
engineered nanomaterials, 独立行政法
人物質・材料研究機 構(茨城県つくば市)、
2012 年 9 月、招待

Jun Kanno, Atsuya Takagi, Yuhji
Taquahashi, Mitsuru Futakuchi*,
Hiroyuki Tsuda**, Akihiko Hirose,
NANOMATERIAL TOXICOLOGY -
IMPORTANCE OF CHRONIC
TOXICITY ASSESSMENT, the 8th
Congress of Toxicology in Developing
Countries (8CTDC) (2012.9.11)
Bangkok, Thailand, poster

高橋祐次、高木篤也、菅野　純、高度に分散性を高めた多層カーボンナノチューブのp53 ヘテロ欠損マウス腹腔内投与による中皮腫発がん、第 27 回発癌病理研究会、2012 年 8 月、伊豆、口演

Jun Kanno, Nanomaterial Toxicity, its Chronic Aspects. The 6th International Congress of Asian Society of Toxicology (2012.7, Sendai) Symposium

髙橋祐次、小川幸男、高木篤也、相磯成敏、今井田克己、菅野純、音響式ダスト発生装置を用いた多層 カーボンナノチューブの全身曝露吸入と肺内負荷量の測定、第 39 回日本毒性学会学 術年会、2012 年 7 月、仙台、一般口演

高橋俊孝、中川ゆづき、豊泉友康、田島恵理、西村哲治、本間正充、山影康次、本間正充；カーボンナノチューブの CHL/IU 培養細胞を用いた染色体異常試験（その 2）：日本環境変異原学会第 41 回大会 (2012.11)

安井学、鴨下渚、本間正充;ライブセルイメージングを用いた多層カーボンナノチューブによる倍数性細胞の発生機序の解明：日本環境変異原学会第 41 回大会(2012.11)

坂本義光, 小縣昭夫, 前野智和, 西村哲治, 広瀬明彦, 小杉有希, 鈴木俊也, 中江大：5種の多層カーボンナノチューブ（MWCNT）のラット腹腔内投与による中皮腫の誘発.第39回日本毒性学会学術年会; 仙台, 2012

Sakamoto Y, Ogata A, Nishimura T, Hirose A, Nakae D. Induction of methothelioma by an intraperitoneal adoministration of 5 different manufactured multi-wall carbon nanotubes.71th Annual Meeting of the Japanese Cancer Association; Sendai 2012

山本行男、坂本義光、大貫文、猪又明子、小縣昭夫、中江大. 多層カーボンナノチューブ投与により誘発したラット中皮腫におけるプロテオーム解析（第二報）. 第 85 回日本生化学会大会; 福岡, 2012.

藤谷知子、大山謙一、中江　大、小縣昭夫、広瀬明彦、西村哲治：マウスにおける多層カーボンナノチューブの催奇形性について、日本毒性学会第 39 回日本毒性学会学術年会; 仙台, 2012

Fujitani T, Ohyama K, Nakae D, Ogata A, Hirose A, Nishimura T. Teratogenicity of multi-wall carbon nanotube in ICR mice. The 6 th International Congress of Asian Society of Toxicology; Sendai, 2012

Kobayashi N, Kawabe M, Furukawa F, Kubota R, Sugimoto N, Hirose A: Evaluation of reproductive and developmental toxicity of multi-wall carbon nanotubes in pregnant mice after tail vein administration. 6th International Congress of Asian Society of Toxicology (ASIATOX-VI) (Sendai, 2012).

小林憲弘, 河部真弓, 古川文夫, 久保田領志, 杉本直樹, 広瀬明彦 (2012): 妊娠ラットを用いた尾静脈内投与による多層カーボンナノチューブの生殖・発生毒性の評価と体内動態. 第 39 回日本毒性学会学術年会 (2012,仙台).

柴田麻美、黒木奈緒、本郷聡子、吉田裕樹、

紺野克彦、広瀬明彦、黒川昌彦、渡辺　渡
有機リン系殺虫剤メタミドホスの周産期曝露によるRSウイルス感染免疫への影響、第60回日本ウイルス学会学術集会、2012.11.13, 大阪、ポスターP1-147

Wataru Watanabe, Hiroki Yoshida, Akihiko Hirose, Katsuhiko Konno, Masahiko Kurokawa Effects of nanoparticles of titanium dioxide on the immune redponse to virus infection. EUROTOX2012, (2012, Stockholm)

Nishimaki-Mogami T, Cui H, Okuhira K, Naito M, Suzuki K, Nishimura T, Hirose A.　Mechanism underlying multiwall carbon nanotube-induced IL-1beta secretion.　EUROTOX 2012 (2012, Stockholm)

**H. 知的財産権の出願・登録状況**（予定を含む）

1. 特許取得（出願中）

発明の名称：ナノ粒子の吸入曝露による発がんリスクマーカーおよびその用途
出願日：平成21年3月24日
出願番号：特願2009-071951
発明者　津田洋幸、二口　充、徐　結苟
特許出願人：公立大学法人名古屋市立大学

発明の名称：PCT 出願「ナノ粒子の吸入曝露による発がんリスクマーカーおよびその用途」
出願日：平成21年9月25日
出願番号：PCT/JP2009/004848
発明者　津田洋幸、二口　充、徐　結苟
特許出願人：津田洋幸

発明の名称：国内優先出願「ナノ粒子の吸入曝露による発がんリスクマーカーおよびその用途」
出願日：平成22年3月26日
出願番号：特願2010-58903
発明者　津田洋幸、二口　充、徐　結苟
特許出願人：公立大学法人名古屋市立大学

2. 実用新案登録

なし

3. その他

なし

別添４

# Ⅱ．研究成果の刊行に関する一覧表

書籍

| 著者名 | 論文タイトル | 書籍全体の編集者名 | 書籍名 | 出版社名 | 出版地 | 出版年 | ページ |
|---|---|---|---|---|---|---|---|
| | | | | | | | |

雑誌

| 著者名 | 論文タイトル | 発表誌名 | 巻号 | ページ | 出版年 |
|---|---|---|---|---|---|
| **Miyazawa K.** | **Synthesis of fullerene nanowhiskers using the liquid–liquid interfacial precipitation method and their mechanical,electrical and superconducting properties.** | **Sci. Technol. Adv. Mater.** | **16** | **13502** | **2015** |
| **Konno T, Wakahara T, Miyazawa K,** | **Synthesis and structural analysis of C60-C70 two-component fullerene nanowhiskers** | **J. Cryst. Growth** | **416** | **41-46** | **2015** |
| 宮澤薫一 | 液ー液界面析出法(LLIP法)によるフラーレンのナノウィスカー・ナノチューブ・ナノシートの合成. | **Journal of the Society of Inorganic Materials, Japan** | **22** | **92-98** | **2015** |
| **Hashiguchi, S., Yoshida, H., Akashi, T., Komemoto, K., Ueda, T., Ikarashi, Y., Miyauchi, A., Konno, K., Yamanaka, S., Hirose, A., Kurokawa, M., Watanabe, W.** | **Titanium dioxide nanoparticles exacerbate pneumonia in respiratory syncytial virus (RSV)-infected mice.** | **Environ. Toxicol. Pharmacol.** | **39** | **879-886. Doi:10.1016/j.etap.2015.02.017** | **2015** |
| **Xu J, Alexander DB, Futakuchi M, Numano T, Fukamachi K, Suzui M, Omori T, Kanno J, Hirose A,** | **Size- and shape-dependent pleural translocation, deposition, fibrogenesis, and mesothelial proliferation by** | **Cancer Sci.** | **105** | **763-9** | **2014** |

| | | | | | |
|---|---|---|---|---|---|
| Tsuda H. | multiwalled carbon nanotubes. | | | | |
| Cui H, Wu W, Okuhira K, Miyazawa K, Hattori T, Sai K, Naito M, Suzuki K, Nishimura T, Sakamoto Y, Ogata A, Maeno T, Inomata A, Nakae D, Hirose A, Nishimaki-Mogami T. | High-temperature calcined fullerene nanowhiskers as well as long needle-like multi-wall carbon nanotubes have abilities to induce NLRP3-mediated IL-1beta secretion. | Biochem Biophy Res Commun | 452 | 593-599 | 2014 |
| Miyazawa K, Hirata C, Wakahara T. | Influence of the solution volume on the growth of C60 nanowhiskers. | J. Crystal Growth | 405 | 68-72 | 2014 |
| Numano T1, Xu J, Futakuchi M, Fukamachi K, Alexander DB, Furukawa F, Kanno J, Hirose A, Tsuda H, Suzui M. | Comparative study of toxic effects of anatase and rutile type nanosized titanium dioxide particles in vivo and in vitro. | Asian Pac J Cancer Prev. | 15(2) | 929-935 | 2014 |
| Xu J, Futakuchi M, Alexander DB, Fukamachi K, Numano T, Suzui M, Shimizu H, Omori T, Kanno J, Hirose A, Tsuda H. | Nanosized zinc oxide particles do not promote DHPN-induced lung carcinogenesis but cause reversible epithelial hyperplasia of terminal bronchioles. | Arch Toxicol. | 88 | 65–75 | 2014 |
| Taquahashi, Y, Ogawa, Y, Takagi, A, Tsuji, M, Morita, K, Kanno, J. | An improved dispersion method of multi-wall carbon nanotube for inhalation toxicity studies of experimental animals. | J Toxicol Sci. | 38(4) | 619-28 | 2013 |
| Honma M, Takahashi T, Asada S, Nakagawa Y, Ikeda A, Yamakage K. | In vitro clastogenicity and phototoxicity of fullerene (C(60)) nanomaterials in mammalian cells. | Mutat Res. | 749 | 97-100 | 2012 |

| | | | | | |
|---|---|---|---|---|---|
| 小林憲弘 | ナノマテリアルの曝露による次世代への影響について考える. | ファルマシア | 48(12) | 1191–1191 | 2012 |
| Matsumoto, M., Serizawa, H., Sunaga, M., Kato, H., Takahashi, M., Hirata-Koizumi, M., Ono, A., Kamata, E., Hirose, A. | No toxicological effects on acute and repeated oral gavage doses of single-wall or multi-wall carbon nanotube in rats. | J Toxicol Sci. | 37 | 463-474 | 2012 |
| Takahashi, M., Kato, H., Doi, Y., Hagiwara, A., Hirata-Koizumi, M., Ono, A., Kubota, R., Nishimura, T., Hirose, A. | Sub-acute oral toxicity study with fullerene C60 in rats. | J Toxicol Sci. | 37 | 353-361 | 2012 |
| Takagi A, Hirose A, Futakuchi M, Tsuda H, Kanno J. | Dose-dependent mesothelioma induction by intraperitoneal administration of multi-wall carbon nanotubes in p53 heterozygous mice. | Cancer Sci. | 103(8) | 1440-4 | 2012 |
| Xu J, Futakuchi M, Shimizu H, Alexander DB, Yanagihara K, Fukamachi K, Suzui M, Kanno J, Hirose A, Ogata A, Sakamoto Y, Nakae D, Omori T, Tsuda H. | Multi-walled carbon nanotubes translocate into the pleural cavity and induce visceral mesothelial proliferation in rats. | Cancer Sci. | 103(12) | 2045-50 | 2012 |
| Tomoko Fujitani,Motoko Hojo,Akiko Inomata,Akio Ogata,Akihiko Hirose,Tetsuji Nishimura,Dai Nakae | Teratogenicity of asbestos in mice | J.Toxicol.Sci.. | 39(2) | 363-370 | 2014 |

| | | | | | |
|---|---|---|---|---|---|
| 宮澤薫一 | 液－液海面分析出法によるフラーレンナノファイバーの合成と成長機構 | ナノファイバー学会誌 | 3(12) | 13-17 | 2012 |
| K. Miyazawa, C. Hirata, R. Kano*, T. Wakahara, H. Takeya, T. Yamaguchi, Y. Takano, J. Tang, Y. Lin and M. Tachibana | Structural characterization of the C60 nanowhiskers heat-treated At-high temperatures for potential superconductor application | Trans. Mat. Res. Soc. Japan | 38(4) | 517-520 | 2013 |
| 広瀬　明彦 | ナノマテリアルの健康影響評価指針の国際動向 | 薬学雑誌 | 133(2) | 175-180 | 2013 |

# Ⅲ. 研究成果の刊行物・別冊

OPEN ACCESS
IOP Publishing | National Institute for Materials Science
Science and Technology of Advanced Materials
Sci. Technol. Adv. Mater. 16 (2015) 013502 (10pp)
doi:10.1088/1468-6996/16/1/013502

Review

# Synthesis of fullerene nanowhiskers using the liquid–liquid interfacial precipitation method and their mechanical, electrical and superconducting properties

**Kun'ichi Miyazawa**

Fullerene Engineering Group, Materials Processing Unit, National Institute for Materials Science, Tsukuba, Ibaraki 305-0044, Japan

E-mail: miyazawa.kunichi@nims.go.jp

Received 27 November 2014, revised 14 January 2015
Accepted for publication 16 January 2015
Published 25 February 2015


**Abstract**

Fullerene nanowhiskers (FNWs) are thin crystalline fibers composed of fullerene molecules, including $C_{60}$, $C_{70}$, endohedral, or functionalized fullerenes. FNWs display *n*-type semiconducting behavior and are used in a diverse range of applications, including field-effect transistors, solar cells, chemical sensors, and photocatalysts. Alkali metal-doped $C_{60}$ (fullerene) nanowhiskers ($C_{60}$NWs) exhibit superconducting behavior. Potassium-doped $C_{60}$NWs have realized the highest superconducting volume fraction of the alkali metal-doped $C_{60}$ crystals and display a high critical current density ($J_c$) under a high magnetic field of 50 kOe. The growth control of FNWs is important for their success in practical applications. This paper reviews recent FNWs research focusing on their mechanical, electrical and superconducting properties and growth mechanisms in the liquid–liquid interfacial precipitation method.

Keywords: fullerene nanowhisker, fullerene nanotube, fullerene nanosheet, fullerene nanofiber, LLIP method, superconductor

## 1. Introduction

Fullerene molecules consist of closed cage-type structures that are composed of carbon atoms. The best-known fullerene is $C_{60}$, which was discovered by Kroto *et al* in 1985 [1]. The second well-known molecule is $C_{70}$, which was also identified in [1]. The $C_{60}$ molecule is analogous to a soccer ball with 12 pentagons and 60 vertices where carbon atoms are located, and has 30 six-membered ring/six-membered ring joints with double bonds of carbon and 60 five-membered ring/six-membered ring joints with single bond of carbon.



Polymerization of $C_{60}$ molecules can occur via [2+2] cycloaddition reactions, which form four-membered rings between adjacent $C_{60}$ molecules. This cycloaddition mechanism involves a change of carbon hybridization from $sp^2$ to $sp^3$ [2].

Various properties of $C_{60}$ have been studied by forming thin films on suitable substrates. Bulk samples can also be prepared by sintering at high temperatures. The [2+2] cycloaddition polymerization of $C_{60}$ molecules is known to occur in the presence of ultraviolet or visible light illumination [3, 4], high-pressure sintering [5–8], and electron beam irradiation [9, 10]. The hardness of high-pressure sintered $C_{60}$ reaches 200–300 GPa [11, 12].

However, fine needle-like crystals (whiskers) comprising $C_{60}$, '$C_{60}$ (fullerene) nanowhiskers ($C_{60}$NWs)', were found in

1468-6996/15/013502+10$33.00

a colloidal solution of lead zirconate titanate (PZT) with $C_{60}$ added [13–15].

Fullerene nanofibers are linear and thin, with diameters less than 1000 nm [16, 17]. Fullerene nanosheets are thin two-dimensional substances. In this paper, we define fullerene nanosheets to be less than 1000 nm in thickness. Fullerene nanofibers and nanosheets can include a variety of fullerene molecules and their derivatives including $C_{60}$, $C_{70}$, $Sc_3N@C_{80}$ [18], $C_{60}[C(COOC_2H_5)_2]$ [19–21] and $(\eta^2\text{-}C_{60})Pt(PPh_3)_2$ [22].

The aspect ratio of fullerene nanofibers is defined to be greater than three [16]. Fullerene nanofibers are described as either non-tubular or tubular [23–27]. Non-tubular crystalline fullerene nanofibers are called fullerene nanowhiskers (FNWs). FNWs with both single-crystal and polycrystalline structures have been reported [53].

Fullerene nanofibers can incorporate either one or multiple types of fullerenes. This enables formation of both monocomponent and multicomponent structures. Examples of monocomponent structures include $C_{60}$NWs, $C_{70}$ (fullerene) nanowhiskers ($C_{70}$NWs), $C_{60}$ or $C_{70}$ (fullerene) nanotubes ($C_{60}$NTs or $C_{70}$NTs), [23, 25, 28], and FNWs composed of $C_{60}[C(COOC_2H_5)_2]$ molecules ($C_{60}[C(COOC_2H_5)_2]$NWs). Examples of multicomponent fullerene nanofibers include two-component $C_{60}$–$C_{70}$ NWs [29], two-component $C_{60}$–$C_{70}$ NTs [23], two-component $C_{60}$–$C_{60}[C(COOC_2H_5)_2]$ NWs [19], and two-component $C_{60}$–$(\eta^2\text{-}C_{60})Pt(PPh_3)_2$ NWs [22]. Figure 1 shows the classification of fullerene nanofibers.

Fullerene nanofibers and nanosheets can be synthesized using the 'liquid–liquid interfacial precipitation (LLIP) method' [30], which has been widely applied [31–38]. In this review, we discuss the LLIP method to synthesize fullerene nanofibers and nanosheets and the applications in which these materials have been investigated.

The terminology 'FNW' represents all needle-like crystals comprising fullerene molecules with diameters less than 1000 nm. The words 'nanorod' and 'nanowire' are replaced with 'nanowhisker' to avoid confusion as was described in review paper [16].

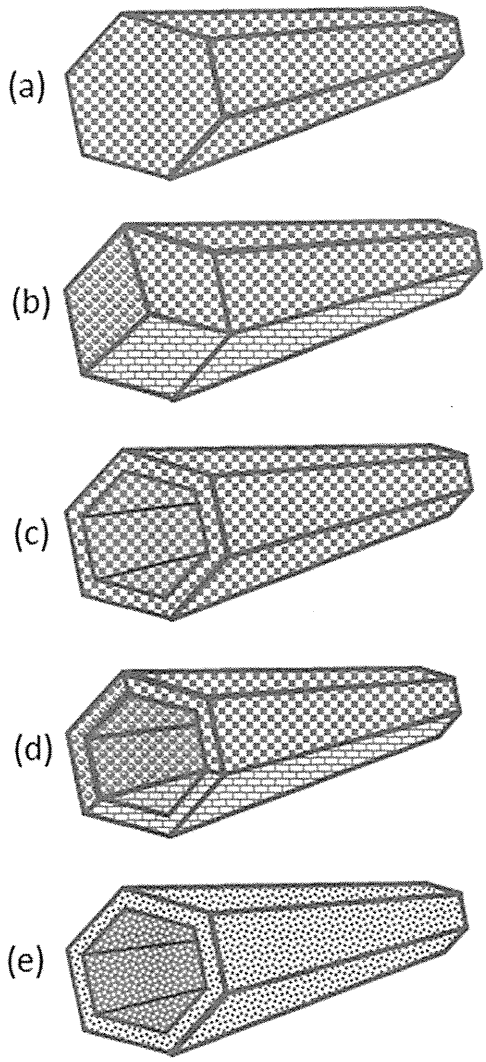


**Figure 1.** Classification of fullerene nanofibers. (a) single-crystal fullerene nanowhisker, (b) polycrystal fullerene nanowhisker, (c) single-crystal fullerene nanotube, (d) polycrystal fullerene nanotube, (e) amorphous fullerene nanotube.

## 2. Synthesis of FNWs

### *2.1. LLIP method*

The LLIP method is commonly used to synthesize fullerene nanofibers and nanosheets [30]. This method relies on diffusion of a poor solvent of fullerenes such as isopropyl alcohol (IPA) into a fullerene-saturated toluene solution. An aliquot of a $C_{60}$-saturated toluene solution is added to a glass bottle. Following this, an appropriate amount of IPA is added gently to the solution to form a liquid–liquid interface [8]. The resulting mixture is kept at ambient temperatures, typically below 25 °C. During the slow mixing of toluene and IPA, the liquid–liquid interface becomes supersaturated in $C_{60}$ and allows nucleation of $C_{60}$NWs to occur. This supersaturated state is maintained as IPA diffuses into toluene and assists in the growth of $C_{60}$NWs. This procedure is named 'static LLIP method' [30, 39]. The glass bottle is kept still in an incubator, where the $C_{60}$NWs self-assemble into a shape similar to a cotton ball. The LLIP method can also be used in combination with ultrasonic mixing, manual mixing, or injection [24, 39, 40]. Ultrasonication induces rapid mixing of good solvents and poor solvents, causing formation of fine fullerene nuclei that grow into fullerene nanofibers or nanosheets.

The static LLIP method can involve either layering a poor solvent onto a good solvent or vice versa, and can be combined with manual mixing, supersonic mixing, mixing by injection of liquid, or ultrasonic mixing of liquid droplets [41]. These methods are collectively named the 'dynamic LLIP method'.

Cha *et al* and Miyazawa *et al* reported the diaphragm LLIP method (DLLIP method), which involves injecting a poor solvent for fullerene into a fullerene solution through a porous membrane [40, 42, 43]. As an example, if IPA is slowly injected into a $C_{60}$-saturated toluene solution through

an anodic aluminum oxide membrane with nanosized pores, vertically grown microtubes of $C_{60}$ are produced. All methods that mix two solvents to form fullerene nanofibers and nanosheets can be classified as LLIP processes.

Using the DLLIP method, the influence of alcohol chain length (methanol, ethanol, and IPA) on the length of $C_{60}$ whiskers was investigated using toluene as a good solvent for $C_{60}$. Amer *et al* reported that the length of $C_{60}$ whiskers decreased when the chain length of the alcohol (poor solvent) increased [44]. The temperatures at which the $C_{60}$ whiskers were grown was not reported; however, the above result suggests that the chain length of the alcohol influences the desolvation energy of solvated $C_{60}$ molecules that governs the rate-limiting process of surface reaction [45].

### 2.2. Growth mechanism of FNWs using the LLIP method

The Young modulus of $C_{60}$NWs has been examined using a transmission electron microscope equipped with an atomic force microscope [46]. The Young modulus of $C_{60}$NWs increases with decreasing diameter [46–49]. This phenomenon is thought to occur because $C_{60}$NWs have a core–shell structure with a porous interior region and a dense surface region [48, 50]. Kizuka *et al* found that $C_{70}$NWs containing solvent molecules had a higher density of lattice defects in their interior regions, which caused a reduction in the Young modulus [51]. Additionally, the Young modulus of $C_{70}$NTs was found to increase with decreasing diameter [25]. These studies conclude that by decreasing the diameter of fullerene nanofibers, crystallinity is increased, which in turn leads to an increase in the Young modulus.

In the LLIP process, FNWs grow from seed crystals [52–54]. The size of the initial $C_{60}$NW nuclei is influenced by the degree of supersaturation of $C_{60}$ in solution, which is determined by the mixing ratio of both good and poor solvents [39]. $C_{60}$NTs grow in both directions along their growth axis from the seed crystals [53, 54]. However, the seed crystals should disappear by the core dissolution mechanism to form a through-hole structure [55].

The re-growth of $C_{60}$NTs was observed in ultrasonically pulverized $C_{60}$NTs [53]. The ultrasonically fractured $C_{60}$NTs have steep wall edges, on which $C_{60}$ molecules accumulate and crystallize [53]. This preferential accumulation of $C_{60}$ in areas with a small radius of curvature, such as the hexagonal vertices, is an important growth mechanism of fullerene nanotubes [53, 54].

The growth of $C_{60}$NWs is influenced by numerous factors, including time, temperature, light, solvent species, the ratio between good and poor solvents, and contained impurity water [39, 56–59]. The growth mechanism of $C_{60}$NWs in $C_{60}$-saturated toluene and IPA has been studied closely. The activation energy of growth (52.8 kJ $mol^{-1}$) was calculated by varying the temperature and measuring the length of $C_{60}$NWs. This value is approximately four times greater than the value obtained for the diffusion of $C_{60}$ in a mixed solution of toluene and acetonitrile (13.1 kJ $mol^{-1}$, 4:1 v/v) [56, 60]. The high activation energy indicated that the growth of $C_{60}$NWs is rate limited by the desolvation process of $C_{60}$ molecules bonded with solvent molecules on the crystal surface.

The dynamic LLIP process involves a fullerene solution being forcibly mixed with a poor solvent for fullerene. This process generates microscopic liquid–liquid interfaces between the fullerene solution and the poor solvent of fullerene, where supersaturated solutions lead to rapid nucleation of fine fullerene crystals. The formation of granular, linear, or sheet fullerene crystal morphologies depends on the growth kinetics, which may be governed by the degree of supersaturation, solvent species, and temperature.

Size control of fullerene nanofibers is critical for practical applications. Wakahara *et al* reported that the diameter of $C_{60}$NWs varied with the size of the glass bottles used in their synthesis. Linear relationships between the area of the liquid–liquid interface and the diameter of $C_{60}$NWs were observed when the total volume of solution was fixed [61]. Changes in the lengths and diameters of $C_{60}$NWs upon varying the solution volume have been examined [62]. These $C_{60}$NWs were prepared by dynamic LLIP in a $C_{60}$-saturated toluene and IPA system. After the initial formation of a liquid–liquid interface by layering an equal amount of IPA on a $C_{60}$-saturated toluene solution, the solution was manually mixed by shaking 30 times. The relationships between solution volume and mean length, diameter and aspect ratio are shown in figures 2(a)–(c) [62]. The aspect ratio, as derived from the *y*-intercepts of figures 2(a) and (b) (5.02 $\mu$m/387 nm) yielded a value of 13.0, almost identical to the value derived from the *y*-intercept of figure 2(c) (13.1). Hence, it is reasonable to consider the size of $C_{60}$NW nuclei can be estimated using the relationships shown in figures 2(a)–(c).

The relationship between the solution volume and number of $C_{60}$NWs per unit volume is shown in figure 2(d). The number density, as calculated from the nominal content of $C_{60}$ and the mean size of $C_{60}$NWs in solution [62], increased as the solution volume decreased. This implies that the volume fraction of liquid–liquid interfaces increases when the solution volume is decreased. A power law relationship ($y = 1.12 \times 10^9 x^{-0.567}$) was fitted to the data with an approximate index of −0.5, showing that the number density of $C_{60}$NW nuclei in solution is inversely proportional to the square root of the solution volume.

A model describing the changes in the liquid–liquid interface upon manual mixing is shown in figure 3. The initial layered interface (figure 3(a)) is assumed to form a sinusoidally modulated interface (figure 3(b)) upon the manual mixing. The amplitude of this interface increases along the height of the glass bottle, a section of this wavefront is highlighted by the blue rectangle (figure 3(c)). This highlighted section is modeled by a cylinder with height $h$, radius $r$, basal area $S$, and volume $V$ (figure 4(a)). The front of the liquid–liquid interface travels vertically with a velocity $v$.

The following equations hold.

$$V = Sh, \tag{1}$$

$$h = pr, \text{ where } p \text{ is a constant,} \tag{2}$$

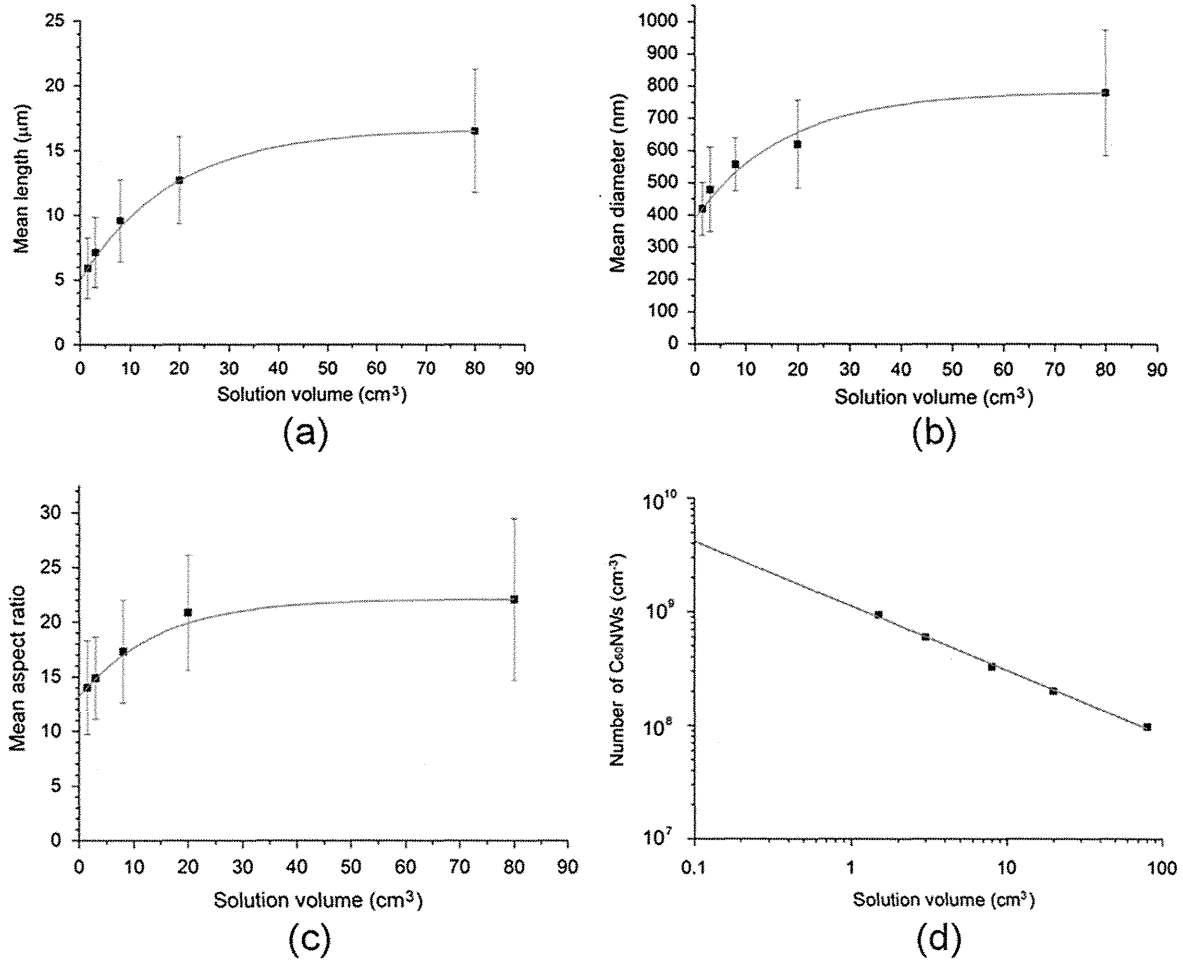


**Figure 2.** (a) Relationship between solution volume and mean length of $C_{60}$NWs. The equation fitted to the data is $y=-11.6\exp(-x/18.7)+16.6$. (b) Relationship between solution volume and mean diameter of $C_{60}$NWs. The equation fitted to the data is $y=-396.6\exp(-x/17.6)+783.7$. (c) Relationship between solution volume and the mean aspect ratio of $C_{60}$NWs. The equation fitted to the data is $y=-9\exp(-x/14.2)+22.1$. (d) Estimated number of $C_{60}$NWs per unit volume plotted versus the solution volume. The equation fitted to the data is $y=-1.12496\times10^{9}\,x^{-0.5674}$. Reprinted from [62], copyright 2014, with permission from Elsevier.

$$V = qS^{3/2}, \text{ where } q = p/\pi^{1/2}. \tag{3}$$

The front of liquid–liquid interface is assumed to move along the height $h$ with a time $t$.

$$t = h/v. \tag{4}$$

As the liquid–liquid interface front moves, interdiffusion between $C_{60}$-satulated toluene solution and IPA occurs (figure 4(b)). If the values of both $t$ and $\Delta r$ are assumed to be small, the area of the interdiffusion zone ($\Delta S$) is approximated as follows:

$$\Delta S = 2\pi r \Delta r. \tag{5}$$

The volume of interdiffusion $\Delta V$ is:

$$\Delta V = h\Delta S. \tag{6}$$

If $\Delta r$ is assumed to be proportional to $(Dt)^{1/2}$ with a coefficient of interdiffusion $D$ [63], it is calculated as in equation (7) with a constant $a$,

$$\Delta r = at^{1/2}. \tag{7}$$

Hence, combining (4), (5), and (7),

$$\Delta S = bh^{1/2}, \text{ where } b = 2\pi ra(1/v)^{1/2}. \tag{9}$$

If $N$ is defined as the number of $C_{60}$NW nuclei per unit volume in the zone of interdiffusion, the mean number of $C_{60}$NW nuclei contained in a unit volume of a cylinder ($\rho$) can be calculated by combining equations (1), (3), (6), and (9):

$$\rho = (Nbq)V^{-1/2}. \tag{12}$$

This model suggests that the mean number density of $C_{60}$NW nuclei is inversely proportional to the square root of the solution volume, which was indeed confirmed experimentally (figure 2(d)).

## 3. Electrical and superconducting properties of $C_{60}$NWs

$C_{60}$NWs display $n$-type semiconducting behavior and are used in a diverse range of applications, including field effect

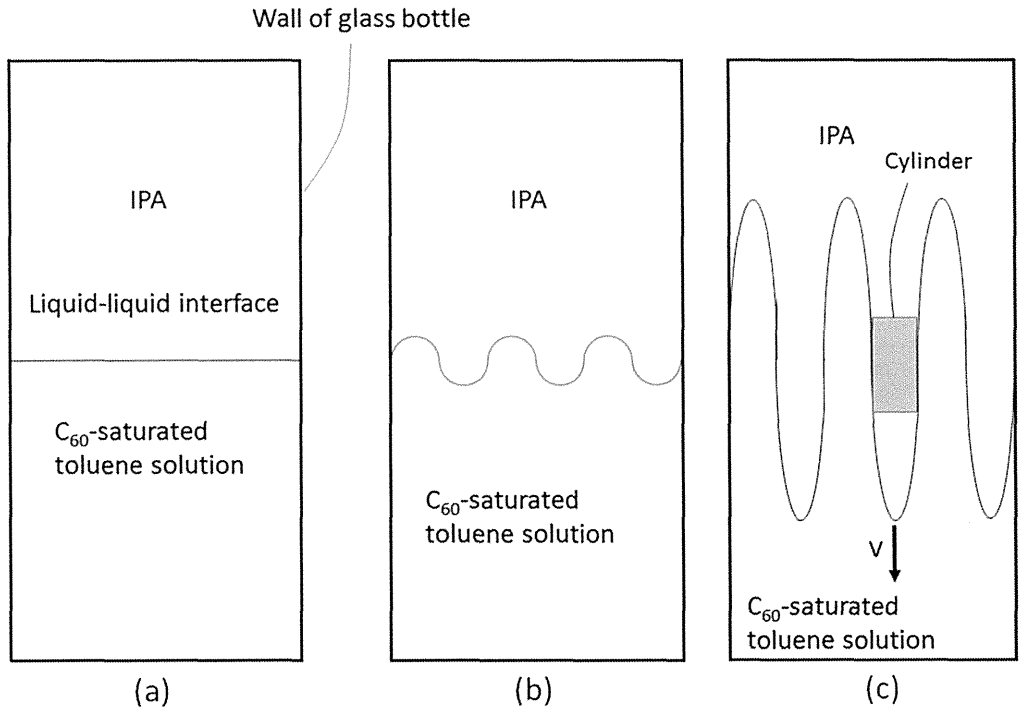


**Figure 3.** Model showing the liquid–liquid interface (a) changing with manual mixing (b). The interface front between the $C_{60}$-saturated toluene solution and IPA is assumed to move with a velocity v along the vertical direction of the glass bottle (c).

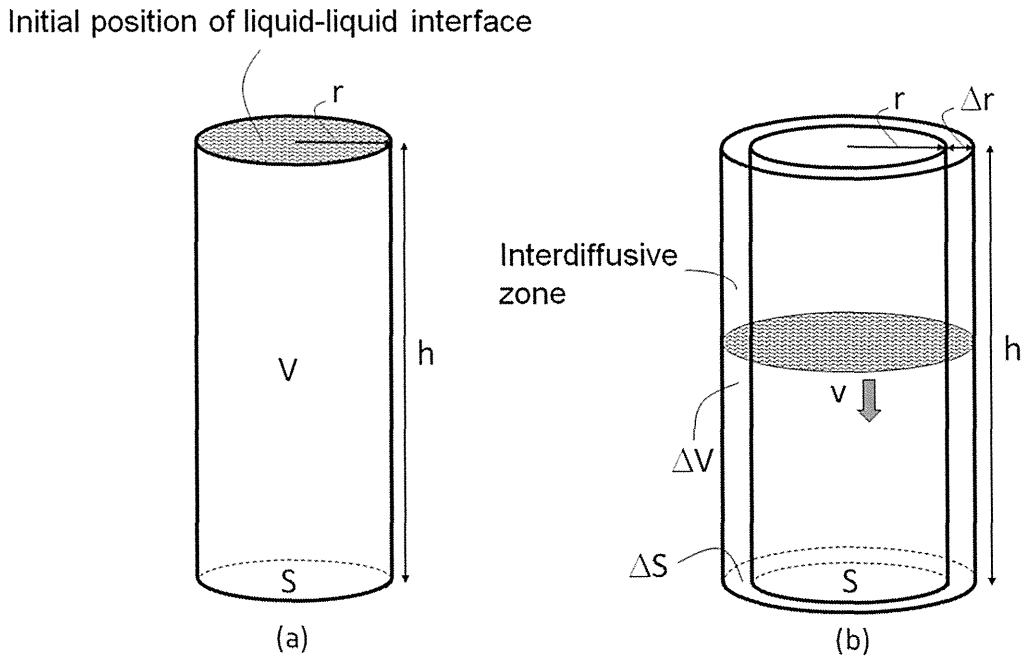


**Figure 4.** Cylindrical model used to calculate the number density N of $C_{60}$NW nuclei for the region of the liquid–liquid interface shown in figure 3(c).

transistors (FETs) [64], solar cells [65, 66], photocatalysts [67], chemical sensors [27], and photosensors [68]. However, Wakahara *et al* recently synthesized ambipolar FETs with $C_{60}$/cobalt–porphyrin hybrid nanosheets using a LLIP method [92].

The carrier mobility of $C_{60}$NWs in a FET was determined to be $2 \times 10^{-2}$ cm$^2$ V$^{-1}$ s$^{-1}$ under vacuum [64]. However, the as-synthesized solution-grown $C_{60}$ needle-like crystals exhibited a very high mobility up to 11 cm$^2$ V$^{-1}$ s$^{-1}$ [69]. As the measured carrier mobility of $C_{60}$NWs, or needle-like crystals of $C_{60}$, depends largely on the measurement conditions (solvent impurities, oxygen impurity, crystal structure, and lattice defects), electrical properties of the materials were investigated under controlled conditions. Only $C_{60}$NWs with clearly defined chemical and structural properties were used.

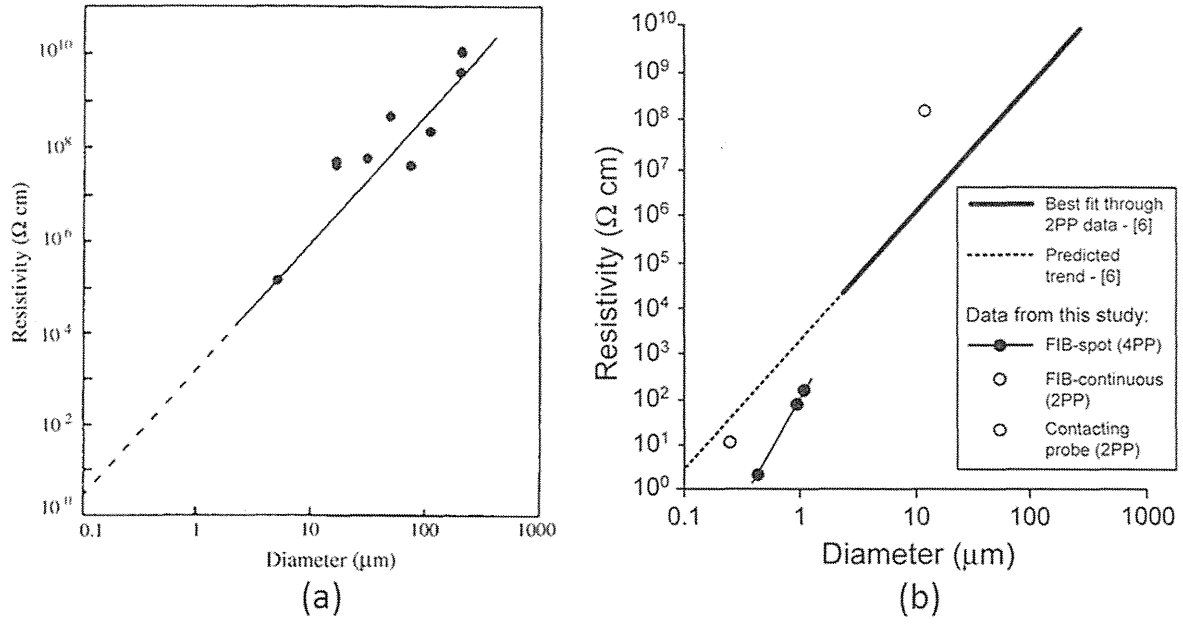


**Figure 5.** Electrical resistivity of $C_{60}$ whiskers measured as a function of diameter. The resistivity measurement was performed by the two-point probe method (2PP) in (a) and by the four-point probe method (4PP) in (b). [6] in the inset of (b) is identical with [70]. FIB stands for focused ion beam. Part (a) reprinted with permission from [70], copyright © 2003 John Wiley & Sons, Ltd. Part (b) reproduced by permission of ECS—The Electrochemical Society from [71]

The electrical resistivity of $C_{60}$ whiskers with diameters greater than 1 $\mu$m (~10–a few hundred micrometers) was measured using a two-terminal method at ambient temperature [70]. The electrical resistivity of the $C_{60}$ whiskers decreased dramatically with decreasing diameter (figure 5(a)). The resistivity of $C_{60}$NWs is expected to be several Ohm centimeters ($\Omega$ cm), based on extrapolation of the curve-fitted data. Subsequently, Larsson *et al* measured the electrical resistivity using a four-point probe method [71]. Figure 5(b) summarizes their results including figure 5(a) [70]. The four-point probe method also showed a decrease in resistivity of $C_{60}$ whiskers with decreasing diameter (FIB-spot (4PP)), figure 5(b)). A $C_{60}$NW with a diameter of 650 nm showed a low resistivity of 3 $\Omega$ cm [71]. The decrease in resistivity with decreasing diameter suggested that $C_{60}$NWs with smaller diameters and shorter $C_{60}$ intermolecular distances are more crystalline and thus have a greater overlap of $\pi$ electrons [70]. Recently, this fact was further confirmed by Barzegar *et al* using thinner $C_{60}$NWs [93]. It was shown that the electrical mobility of as-grown $C_{60}$NWs with diameters less than 300 nm increases with decreasing the diameter of $C_{60}$NWs [64, 93–95].

If the line measured using the four-point probe method is extrapolated to a diameter of 100 nm in figure 5(b), the resistivity will decrease to the order of $10^{-3}$ $\Omega$ cm. This result suggests that $C_{60}$NWs may exhibit metallic conductivity when their diameters are sufficiently small. Xu *et al* showed that $C_{60}$NWs are conductive only if the surface is not covered by oxygen [72].

To determine the electrical properties of a semiconductor, it is necessary to measure the temperature dependence of electrical conductivity. Ji *et al* performed these measurements using $C_{60}$NWs with either a face-centered cubic (fcc) or a hexagonal closed packed (hcp) structure [73]. The fcc $C_{60}$NW displayed higher electrical conductivity than did the hcp $C_{60}$NW. This result confirms that the crystal structure influences the electrical properties of $C_{60}$NWs. However, the effect of solvent molecules contained in the hcp $C_{60}$NW is still under some debate. If $C_{60}$ molecules adopt a closely packed structure, a greater overlap between $\pi$ electrons would lead to higher electrical conductivity in these $C_{60}$NWs [70, 73].

Carbon superconductors have been investigated for many years. The superconductivity of graphite ($C_8$) specimens doped with alkali metals, including K (superconducting transition temperature ($T_c$) < 0.55 K [74], 0.128–0.198 K [75]), Cs ($T_c$ = 0.020–0.135 K [74]), and Rb ($T_c$ = 0.023–0.151 K [74]) has been reported. Graphite superconductors such as $C_6Ca$ ($T_c$ = 11.5 K) and $C_6Yb$ ($T_c$ = 6.5 K) were also synthesized [76]. $C_{60}$NWs can be transformed into glassy carbon nanofibers by heat treatment [77–79]. When heated to 3000 °C, $C_{60}$NWs transform into carbon nanofibers with up to 17 graphene layers [77]. The number of stacked graphene layers increases with increasing temperature between 2000 and 3000 °C [77]. Those $C_{60}$NWs heated at high temperatures with developed graphitic ribbons are promising materials that may exhibit superconductivity if doped with alkali metals and alkaline-earth metals. In addition, the high-temperature-treated $C_{60}$NWs become electron emission tips showing striped patterns that reflect the atomic structure of the crumpled graphitic layers [78, 79]. However, since long amorphous carbon nanofibers prepared by high-

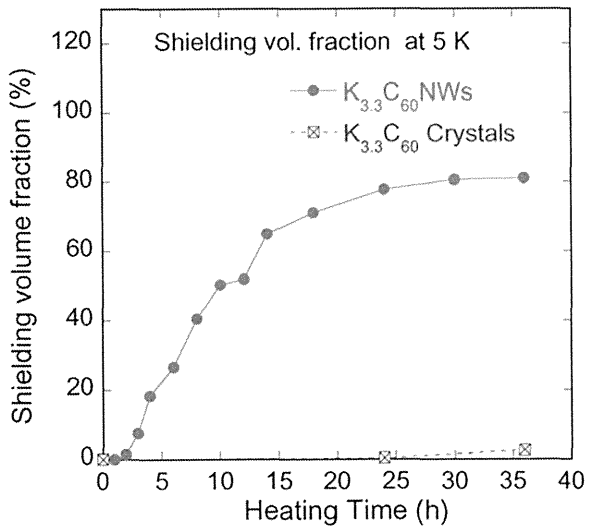


**Figure 6.** Shielding volume fractions in K-doped $C_{60}$NWs and K-doped $C_{60}$ crystal powder (reprinted from [87]).

temperature heat treatment of $C_{60}$NWs showed cytotoxicity like long multiwall carbon nanotubes [96], special care will be necessary in the practical uses of the glassy carbon nanofibers.

In 2004, boron-doped diamond was observed to exhibit superconductivity ($T_c \approx 4$ K) [80]. Takano *et al* found that the $T_c$ of a boron-doped diamond film was 7.4 K [81].

Hebard *et al* discovered that $C_{60}$ doped with potassium (K) exhibited superconductivity [82]. A superconducting transition temperature ($T_c$) of 18 K was observed for both K-doped $C_{60}$ films and bulk samples. Tanigaki *et al* reported the highest $T_c$ value of 33 K in $Cs_2Rb_1C_{60}$ powder [83].

Of the three known phases of K-doped $C_{60}$ (fcc ($K_3C_{60}$), body-centered tetragonal (bct) ($K_4C_{60}$), and body-centered cubic (bcc) ($K_6C_{60}$)), only the fcc phase exhibits superconductivity [84]. Although $C_{60}$NWs that are grown in solution display a solvated hexagonal structure, they transform into an fcc structure upon drying and removal of the internal solvent molecules [85]. Hence, these fcc $C_{60}$NWs should be superconducting if doped with alkali metals [15]. $C_{60}$ nanotubes were doped with Li, Na, and K, and the crystal structures were examined using Raman spectroscopy [86]. Superconductive $C_{60}$NWs were also successfully fabricated by doping with K [87, 88]. Although the $T_c$ value (17 K) of the K-doped $C_{60}$NWs with a nominal composition of $K_{3.3}C_{60}$ was lower than the reported value of 18 K [82], the superconducting, shielding volume fraction was as high as 80%, and the critical current density $J_c$ was more than $3 \times 10^5$ A cm$^{-2}$ under 50 kOe [87, 88], although the doping was performed at 200 °C for 24 h. The shielding volume fraction of the K-doped $C_{60}$ crystal powder was less than 1% when doped using the same process (figure 6). The high shielding volume fraction in the K-doped $C_{60}$NWs may allow for light, flexible, and recyclable superconducting carbon cables. Initially, the superconducting shielding volume fraction of K-doped $C_{60}$ crystals was at most 35%, even after prolonged heat treatment (20 days) at temperatures up to 250 °C [89].

Efforts to increase the $T_c$ value of alkali-doped $C_{60}$NWs are continuing. Values up to 26 K have been achieved by doping with Rb [90]. The volume fraction of Rb-doped $C_{60}$NWs was approximately five times greater than that of Rb-doped $C_{60}$ powder. As Rb is an abundant alkali metal like the other common metals such as copper, lead, or zinc [91], lightweight Rb-doped $C_{60}$NWs are expected to find use in a variety of superconducting applications, including motor cars, cables for power delivery, and wind generators.

## 4. Summary

A variety of fullerene nanofibers and nanosheets have been synthesized using LLIP methods. These materials have found use in a wide range of applications, including solar cells, chemical sensors, photo sensors, photocatalysts, and ambipolar field-effect transistors. The synthesis of $C_{60}$NWs using a dynamic LLIP method with a $C_{60}$-saturated toluene solution and IPA suggests that nucleation is governed by the volume of the liquid–liquid interface produced by interdiffusion between the two solvents.

Alkali-metal-doped $C_{60}$NWs are the first carbon fibers to display superconductivity while being lightweight and flexible. K- or Rb-doped $C_{60}$NWs are promising superconductors with $T_c$ values that are higher than those of any other practically used metal superconductors. Additionally, they are composed of non-toxic, abundant, and recyclable elements. Fullerene nanomaterials show great promise for a variety of applications in electrical and optical fields.

## Acknowledgments

This research was supported by the Health and Labour Sciences Research Grants (H24-Chemistry-Shitei-009) from the Ministry of Health, Labour and Welfare of Japan, the JST Strategic Japanese-EU Cooperative Program 'Study on managing the potential health and environmental risks of engineered nanomaterials', the Center of Materials Research for Low Carbon Emission of the National Institute for Materials Science, and the Japan Society for the Promotion of Science KAKENHI Grant No. 26600007.

## References

[1] Kroto H W, Heath J R, O'Brien S C, Curl R F and Smalley R E 1985 $C_{60}$: buckminsterfullerene *Nature* **318** 162–3
[2] Okada S, Saito S and Oshiyama A 1999 New metallic crystalline carbon: three dimensionally polymerized $C_{60}$ fullerite *Phys. Rev. Lett.* **83** 1986
[3] Rao A M *et al* 1993 Photoinduced polymerization of solid $C_{60}$ film *Science* **259** 955–7
[4] Kato R and Miyazawa K 2012 Raman laser polymerization of $C_{60}$ nanowhiskers *J. Nanotechnol.* **2012** 101243